Using Alkylammonium Salt to Enhance the Adsorption Potential for Ca-Montmorillonite Clay to Remove Color Effluent from Wastewater

Dunya Edan AL-Mammar[1], Rasha Tariq Salim[2*], and Noor Hussein AL-Shammari[1]

[1]*Department of Chemistry, College of Science, University of Baghdad, Al Jadriya Street, Baghdad 10071, Iraq*

[2]*College of Pharmacy, Uruk University, Al-Wahda, 52 Street, Baghdad 00964, Iraq*

* Corresponding author:

tel: +964-7713519465
email: rashatariq46@gmail.com

Abstract: *Ca-montmorillonite raw clay (Ca-M) was modified using two different alkylammonium salts, tetramethylammonium iodide (MT) clay, tetrabutylammonium iodide (BT) clay, and used as an adsorbent to remove Biebrich scarlet (BS) dye from wastewater in batch mode. Clay samples were analyzed using an atomic force microscope (AFM), Fourier transform infrared spectroscopy (FTIR), and X-ray diffraction (XRD). The effects of operating parameters affecting the adsorption of BS dye onto clay samples were studied, such as clay weight, adsorption period, initial BS concentration, temperature, and pH. The experimental data were analyzed using Langmuir and Freundlich adsorption isotherm models; the obtained values of correlation coefficient R^2 showed that the adsorption followed the Freundlich isotherm model. Thermodynamic data reveal that the adsorption of BS dye onto BT and MT clay samples is exothermic and occurs spontaneously with a decrease in disorder. In contrast, the adsorption of this dye onto raw clay is endothermic and occurs spontaneously with an increase in disorder. The lower values of enthalpy change refer to the adsorption process as physisorption type. The results of kinetics analysis for the adsorption process showed that the pseudo-second-order model was more suitable to represent the adsorption process than the pseudo-first-order model.*

Keywords: *Ca-montmorillonite; clay; tetramethylammonium iodide; tetrabutylammonium iodide; adsorption*

■ INTRODUCTION

Recent decades have seen a rapid increase in industrial activity, producing enormous amounts of wastewater and raising concerns about water pollution [1]. Wastewater has a strong smell. It contains a lot of suspended matter, nitrogenous materials, and organic waste that is resistant to treatment; these characteristics are typically assessed by chemical oxygen demand. It is concerning that, especially in low-income nations, this toxic effluent is frequently dumped carelessly into rivers and lakes [2]. Significant risks to human health are associated with the accumulation of hazardous water contaminants in living organisms and other environmental media. Technologies and materials that are accessible, easy to use, environmentally benign, transportable, economically efficient, and chemically robust are desperately needed to meet the world's massive demand for clean water. Globally, biological systems, food chains, the economy, and the environment are all negatively impacted by pollutant toxicity [3]. Significant environmental issues are brought on by the numerous dyes found in wastewater, which also contain mutagenic and carcinogenic substances like metals. Because dyes are resistant to light, heat, chemicals, and water; they are visible even at low concentrations, making them challenging to biodegrade in the environment [4]. Biebrich scarlet (BS) dye is widely used in a variety of industries, including paper, cotton, silk, and wool [5], so it is hazardous and non-biodegradable, putting human health and aquatic life at risk [6]. Although these dyes are dangerous, the risks associated with anionic dyes are more severe and include dermatitis, bladder damage, cancer, and asthma [7]. Different treatment methods and techniques to overcome the problem of dye removal

from wastewater include chemical oxidation and membrane, filtration, microbiological degradation, and adsorption [8].

A variety of treatment techniques have been refined to remove colors from industrial effluents. For example, biological therapy, membrane separation, aerobic coagulation, oxidation, and electrochemical procedures are widely used. However, the adsorption approach is regarded to be one of the frequently used techniques for the removal of harmful organic and inorganic chemicals due to its simplicity, viability, and capacity for effective adsorption [9]. Finding cheap and efficient adsorbents such as fly ash, peat, wood powder sawdust composite, coir pith, and lignin has become increasingly focused on contemporary times. The main component of bentonite is expandable montmorillonite clay [4]. There is an extensive range of clay minerals and clays that can be used as the best adsorbents. Two main categories of clays are kaolin and montmorillonite, but there are other subtypes of clay that their chemical compositions have been identified in relation to the main classification [10].

Montmorillonite is employed extensively because of its low cost, plentiful reserves, large specific surface area, excellent cation exchangeability, and potent adsorption advantage. Because of its positive charge, the cationic surfactant can increase the distance between the layers of montmorillonite by exchanging ions with the cations between them in weakly acidic conditions. Additionally, its hydrophilic qualities can be changed to organophilic ones by modifying its surfactant, which increases the material's ability to adsorb organic contaminants. This is because organic molecules are hydrophobic, making it difficult for molecules on the surface of montmorillonite to form hydrogen bonds with them [11]. The structure of montmorillonite clay is a 2:1 type of clay mineral, which consists of two sheets of silica tetrahedra sandwiching a sheet of alumina octahedra. Between the 2:1 layers, an interlayer space of about 1–2 nm or more contains exchangeable cations, such as sodium, calcium, and potassium, as well as water molecules [12].

In this research, Ca-montmorillonite was used due to its promising properties, such as large surface area and high cation exchange capacity. Thus, it can be used as an effective adsorbent to remove BS dye and treat wastewater. Modification leads to unique properties of clay. The modification carried out two types of salts, tetramethylammonium iodide (MT), and tetrabutylammonium iodide (BT), due to their low cost and ease of processing. They also enhance the adsorption capacity of clay samples to the adsorbed dye. The adsorption process is one of the most widely used techniques for eliminating contaminants and colorants from wastewater due to its many benefits: low cost and energy consumption, easy operation, reduced initial investment needs, and increased efficiency compared to conventional and non-conventional approaches.

■ EXPERIMENTAL SECTION

Materials

The BT was at a concentration of 98.0% from the company BDH, and MT was from Fluka AG, Buchs SG. The BS dye was at a concentration of 99.0% from BDH chemicals. BS or Acid Red 66 dye is an anionic water soluble dye with chemical formula $C_{22}H_{14}N_4Na_2O_7S_2$ [13]. It has IUPAC name as sodium-6-(2-hydroxynaphthylazo)-3,4-azodibenzenesulfonate, molar mass 556.48 g/mol; its maximum wavelength is 506 nm [14]. The chemical structure of BS dye is shown in Fig. 1 [15].

Instrumentation

The physical assessment was analyzed using atomic force microscopy (AFM 2022, Nanosurf, and Switzerland). FTIR (Shimadzu-8400, Japan) was utilized in this study to analyze the vibrations of the synthesized compounds. Structural assessment of the clay samples was characterized using an XRD diffractometer (Shimadzu XRD-6000, Japan).
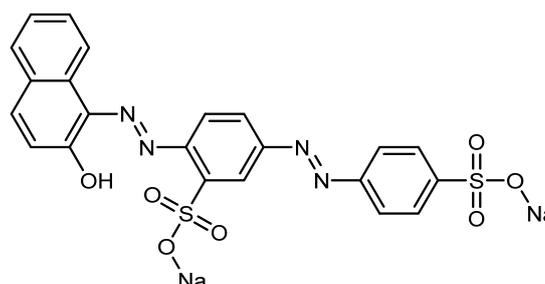

Fig 1. Chemical structure of BS dye

Procedure

Adsorbents preparation

Ca-Montmorillonite clay (Ca-M) was supplied by a state company for mining industries in Baghdad, Iraq. The cation exchange capacity CEC for the pure Ca-M was 65 mg/100 g, and its mesh size was 75 mm. The mineral compositions for this clay are shown in Table 1. This clay was modified using two alkylammonium salts: BT and MT. These two salts have been purchased from Fluka. The Ca-M was initially washed several times with distilled water to remove suspended impurities and then dried at room temperature. After that, 10 g of clay was dispersed in 100 mL of each of BT and MT, and the mixture was stirred for 2 h at 50 °C, where the clay loaded with both BT and MT was filtered and washed with a sufficient amount of distilled water. The produced clay was then dried for 48 h and stored in a dry place for adsorption studies [4].

Preparation of BS dye

To prepare a stock solution of 1000 mg/L BS dye, 1 g of the pure dye was dissolved in 1 L of distilled water. This solution was then diluted to obtain different 10, 20, 30, 40, and 50 mg/L concentrations. The dye concentration at equilibrium was determined using UV-vis spectrometer type (Shimadzu UV-1800, Japan) at λ_{max} 506 nm.

Adsorption experiments

The adsorption experiments for BS dye onto clay and modified clays have been implemented using the batch equilibrium method. A certain weight of clay samples was added to a 25 mL BS dye solution in a 100 mL conical flask. The mixture was stirred by a water bath with thermostat type JTYS-1000 China at a predetermined speed, specific time, and temperature. Then, the solution was centrifuged for 5 min at 4000 rpm to remove the supernatant; the residual BS dye concentration was estimated using a UV-vis spectrophotometer. The removal percentage R% for BS dye and the amount of the adsorbed dye (q_e) in mg g^{-1} were calculated by Eq. (1) and (2) [16];

$$q_e = \frac{V}{M}(C_i - C_e) \tag{1}$$

$$R\% = 100\left(\frac{C_i - C_e}{C_i}\right) \tag{2}$$

where C_i and C_e are the initial concentration and concentration at equilibrium (mg/L). M and V are the weight of clay samples (g) and the working solution (L) volume, respectively.

■ RESULTS AND DISCUSSION

Characterization of the Adsorbents

AFM analysis

The AFM examination provided information about the distribution of cumulating granularity for the clay samples and three-dimensional photographs of the granules' surface topography [17]. Fig. S1 displays the surface derived from method images as well as the granularity cumulating distribution for measurements related to AFM. The mean diameter of the particles is determined to be 257.6, 59.12, and 344.1 nm for BT, MT, and Ca-M clay samples, respectively.

FTIR spectra

FTIR spectra of BT, MT, and Ca-M in the range 400–4000 cm^{-1} are represented in Fig. S2(a), S2(b), and S2(c), respectively. The bands at 3435, 3458, and 3425 cm^{-1}, with the bands at 1635, 1637, and 1649 cm^{-1}, are the stretching and bending vibrations for the hydroxyl groups of water molecules present in the three samples BT, MT, and Ca-M, respectively. The transmission peak was observed in 3618 and 3630 cm^{-1} due to the hydroxyl group bonded with Al^{3+} cations of Ca-M and MT, respectively. The Si–O stretching band can be observed at 1323 cm^{-1} of BT. The bands 922, 916, and 914 cm^{-1} indicate Al–O–Al bending for BT, MT, and Ca-M, respectively. The peaks observed in 839, 833, and 839 cm^{-1} for BT, MT, and Ca-M belong to Al–O–Mg bending. The bands 795 and 797 cm^{-1} were assigned to disordered silica (SiO$_2$) polymorphs for the three clays, respectively. Furthermore, the bands 694.33 cm^{-1}

Table 1. Mineral compositions for Ca-M

Constituent	SiO$_2$	Al$_2$O$_3$	Fe$_2$O$_3$	CaO	Na$_2$O	K$_2$O	MgO	TiO$_2$	MnO	P$_2$O$_5$	LOI
Wt.%	52.122	12.781	4.098	7.660	0.622	0.567	3.044	0.874	0.026	0.458	16.110

for BT and MT and 692.40 cm^{-1} for Ca-M correspond to quartz. Also, bands 532, 519, and 523 cm^{-1} for Si–O bending of three clays, respectively [18]. The C–H bending vibration in N$^+$–CH$_2$ and N$^+$–CH$_3$ were observed between 1402–1469 cm^{-1} for BT. A slight contribution of the butyl chain was also observed in the region of 2871–2958 cm^{-1} due to the hygroscopic character of the cationic surface. New bands at 3281, 3366, and 3387 cm^{-1} arise from the moisture for BT, MT, and Ca-M, respectively [19].

XRD spectra

XRD diagrams are represented in Fig. S3(a), S3(b), and S3(c) for BT, MT, and Ca-M, respectively. The diffraction peaks at 14.949, 23.041, 29.371, and 29.513° indicate that the BT consists of Ca$_3$O$_5$Si, and the peaks at 9.797, 17.664, and 26.985° correspond to the presence of SiO$_2$ zeolite (Fig. S3(a)). While peaks for MT 15.781, 19.487, 31.872, 35.975, and 41.219° are attributed to the existence of Al$_2$(SiO$_4$)O, while 29.520 and 48.676° belong to presence of CaCO$_3$. Also, peaks 22.638, 32.304, 52.164, and 54.438° indicate the potassium molybdenum K$_9$Mo$_6$O$_{17}$ compound (Fig. S3(b)). Fig. S3(c) exhibited firm diffraction peaks at 6.438, 9.110, 21.131, 26.953, 39.893, 50.746, and 60.796° indicating that the Ca-M mainly consists of SiO$_2$ (quartz) and the peaks at 29.624, 36.297 and 47.833° corresponds to the presences of CaCO$_3$ [20].

Adsorption Experiments

Effect of clay sample weight

The effect of clay sample weights on BS dye removal was studied using various amounts of clay samples from 0.05 to 0.25 g into 25 mL of 10 mg/L BS dye solution at 298 K, 150 rpm shaking speed and pH = 7. Fig. 2 shows that the values of R% increased from 30.9, 28.6, and 4.3% to 94.2, 89.2, and 11.2% when the clay sample BT, MT, and Ca-M increased, respectively. This increase would be attributed to the increase in both surface area and active adsorption sites for the adsorbent [8,21]. Therefore, 0.2 g of clay samples were selected as an optimum weight for the adsorption experiments.

Effect of adsorption period

The impact of varying the BS dye adsorption period from 5 to 80 min was investigated by preserving other parameters, such as pH 7, a beginning BS concentration of 10 mg/L, the weight of 0.2 g of clay samples, and a shaking speed of 150 rpm at 298 K. As shown in Fig. 3, the maximum dye removals R% for BT, MT, and Ca-M were 92.3, 82.0, and 34.6%, which were attempted after 60 min as an adsorption period. The rapid adsorption in the region may be due to its expansion of active adsorption sites provided by large electron-donating functional groups. After this period, there is no noticeable increase in adsorption because the adsorbates
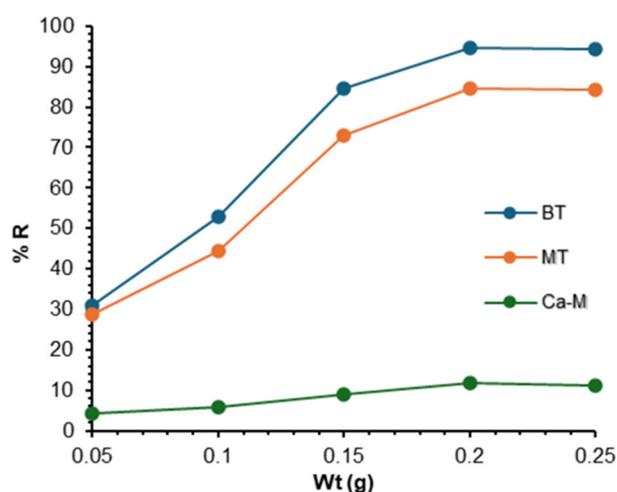
Fig 2. Effect of clay sample weight on the R% of BS dye
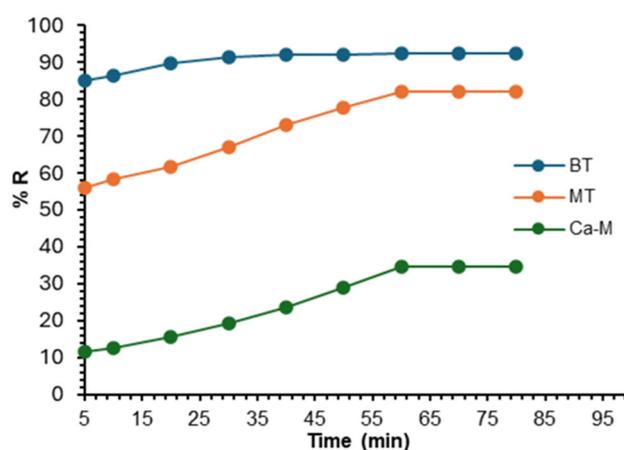
Fig 3. The impact of the adsorption period on the R% of BS dye

have already occupied and consumed the binding sites on the dye surface [22]. The equilibrium adsorption time was reported to be 60 min.

Effect of initial BS concentration

The following experimental settings were used to investigate the effect of initial BS concentration on adsorption at the dye concentrations ranging from 10, 20, 30, 40, and 50 mg/L for clay sample weight: 0.2 g, pH of 7 at 298 K, adsorption period of 60 min, and shaking speed of 150 rpm. Fig. 4 shows that the BS dye removal efficiency decreased with increasing BS dye concentration from 88.28 and 79.05% to 46.45 and 45.98% for the BT and MT samples because the adsorption sites on the adsorbent surface have become saturated [23]. For the Ca-M sample, the dye removal efficiency increases with increasing initial BS concentration. This may be related to the fact that, as the initial BS concentration increases, the interaction forces that are important to overcome the mass transfer resistance between the dye and clay molecules are enhanced [24].

Effect of temperature

The influence of temperatures was determined at the temperature range from 288 to 328 K, 0.2 g clay samples weight per 25 mL of 10 mg/L BS dye solution concentration for 60 min and 150 rpm. Fig. 5 shows that the amount of adsorbed BS dye q_e values using BT and MT samples increases with increased temperature. The temperature affects the adsorbent's efficacy; with rising temperatures, the number of adsorption active sites and the mobility of the dye molecules both increase, resulting in directly proportionate increases in adsorption during the endothermic adsorption process [25-26]. The value of q_e decreased with increased temperature when Ca-M was used as an adsorbent surface. This may be due to a weak adsorption interaction between dye molecules and the active sites in the raw clay surface. The obtained result suggested that the adsorption of BS dye onto raw clay samples can be categorized as an exothermic process [27].

Effect of pH

The impact of pH in the removal of BS dye using clay samples as adsorbents was carried out in the pH range of 2.5–10 while keeping other adsorption conditions. Fig. 6 illustrates that as the values of pH change from 2.5 to 10
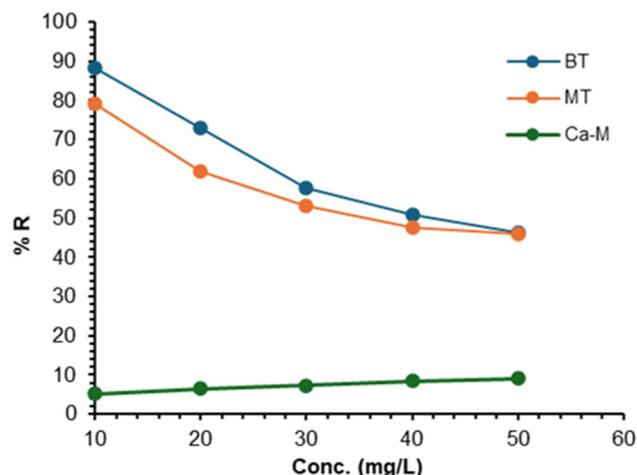

Fig 4. Removal percentage of BS dye as a function of its concentrations
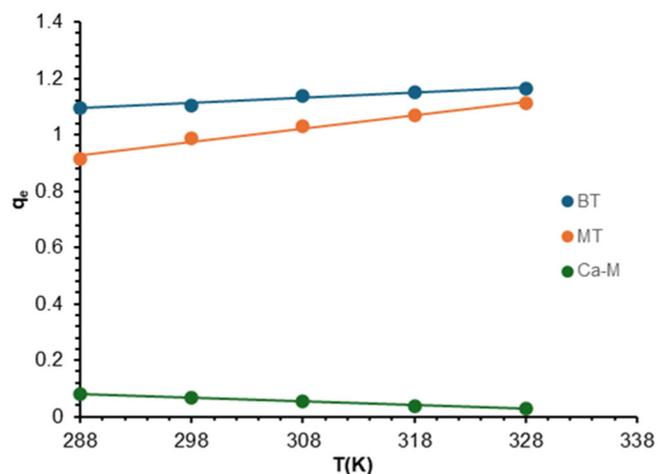

Fig 5. Impact of temperature on the adsorption of BS dye onto clay samples
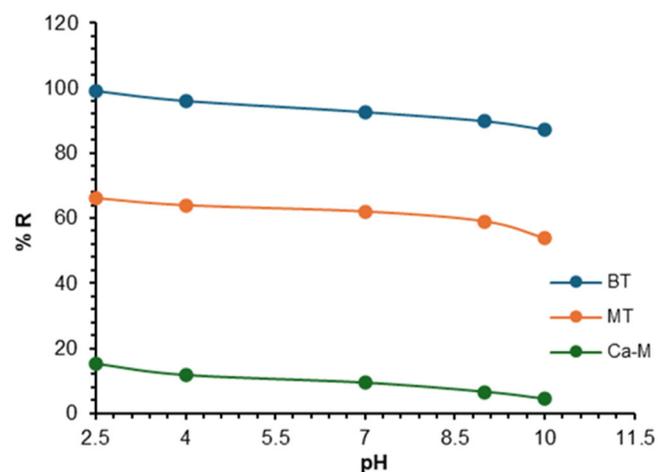

Fig 6. The impact of starting pH on R% values for the BS dye

when the three samples were used as adsorbents, then there is a significant decline in the R% values from 99, 65, and 15% to 87, 53, and 4%, respectively. This may be related to a strong electrostatic interaction between the positively charged H^+ for the adsorbent surface and the adsorbate. On the other hand, when the pH value increases (basic range), there is competition between the extra HO^- in the solution and the anionic ions of BS dye [28].

Adsorption Isotherm Models

Langmuir isotherm model

Langmuir isotherm relies on the development of homogeneous and uniform adsorption sites. The Eq. (3) displays the linear forms of this isotherm [29];

$$\frac{C_e}{q_e} = \frac{1}{K_L q_m} + \frac{1}{q_m} C_e \qquad (3)$$

where C_e represents the adsorbate's equilibrium concentration (mg/L), q_m maximum adsorption capacity of the mono-layer coverage (mg/g), K_L Langmuir isotherm constant (L/mg), and q_e the quantity of adsorbate that adsorbed per g of the adsorbent at equilibrium (mg/g). Fig. 7 displays the Langmuir isotherm plots for the adsorption of BS dye onto BT, MT, and Ca-M clay samples. Table 2 contains a list of the Langmuir estimated parameters and the separation factor R_s values for the 10 mg/L BS dye adsorption onto BT, MT, and Ca-M samples at various temperatures, which were determined using the Eq. (4);
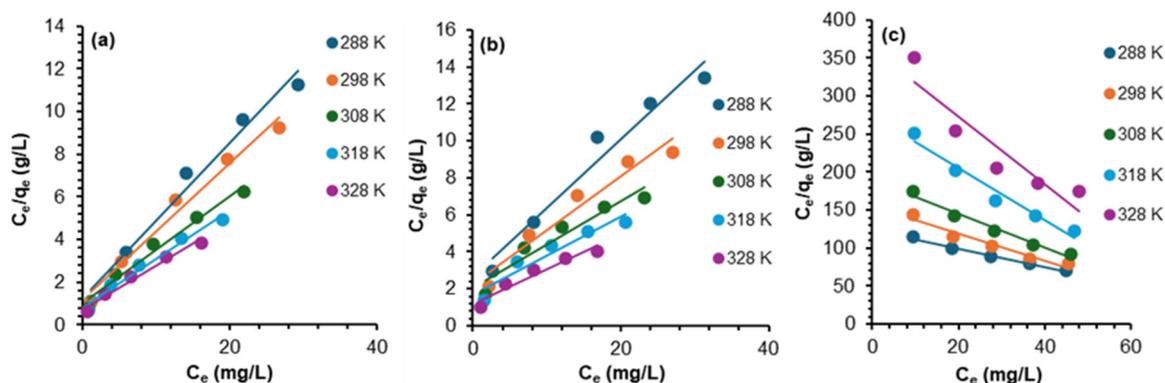

Fig 7. Langmuir isotherms of BS dye at different temperatures on (a) BT, (b) MT, and (c) Ca-M clay samples

Table 2. Langmuir constants and R_s values for the adsorption of BS dye onto BT, MT, and Ca-M clay samples at different temperatures

Adsorbents	Temperature (K)	q_m (mg/g)	K_L (L/mg)	R^2	R_s
BT	288	2.726281	0.306997	0.9802	0.245702
	298	3.125000	0.275150	0.9786	0.266560
	308	3.958828	0.253793	0.9747	0.282651
	318	4.409171	0.271422	0.9769	0.269236
	328	4.878049	0.289425	0.9759	0.256789
MT	288	2.752270	0.143087	0.9598	0.411376
	298	3.432887	0.127461	0.9447	0.439635
	308	4.264392	0.115894	0.9184	0.463190
	318	4.752852	0.124993	0.9088	0.444459
	328	5.347594	0.158273	0.9312	0.387187
Ca-M	288	0.826925	0.009774	0.9889	0.910958
	298	0.562493	0.011487	0.9483	0.896968
	308	0.443636	0.011841	0.9770	0.894129
	318	0.293651	0.012463	0.9617	0.889177
	328	0.224447	0.012298	0.8600	0.890491

$$R_s = \frac{1}{1 + K_L C_i} \qquad (4)$$

The value of R_s provides information about the nature of the adsorption process to be either favorable if $(0 < R_s < 1)$, linear if $R_s = 1$, and unfavorable if $R_s > 1$. As shown in Table 2, the values of R_s lie between 0 and 1 for all adsorbents, indicating that the adsorption process is favorable [30]. The marked increase in the values of monolayer capacity q_m at different temperatures for both modified clay BT and MT refers to that the surface modification of the raw clay achieving the compatibility among the hydrophilic clay layers with hydrophobic alkyl ammonium salts. Also, these salts improve the wetting of the clay layer, leading to enhanced BS dye uptake by these modified clays [31]. Table 3 compares BS dye's prior maximum adsorption capacities with various adsorbents.

Freundlich isotherm model

This model addresses a multilayer heterogeneous energy surface and non-ideal, reversible adsorption [40]. This model's linear form is described in the Eq. (5) [41];

$$\ln q_e = \ln K_{Fr} + \left(\frac{1}{n_f}\right) \ln C_e \qquad (5)$$

where n_f is a constant that depends on the adsorbate nature and temperature, C_e (mg/L) is the equilibrium concentration, and K_{Fr} is Freundlich constant indicated to adsorption capacity. The Freundlich constants were obtained from the intercept and slope of the graph between $\ln q_e$ and $\ln C_e$, as shown in Fig. 8. Table 4 contains the calculated Freundlich constants values for BS dye adsorption onto clay samples. When the value of $1/n$ is below one, it indicates normal adsorption; if it is above one, it indicates cooperative adsorption [42]. It was evident from Table 4 that the values of $1/n > 1$ indicate that the sorption of BS dye onto both BT and MT samples is favorable, while the Ca-M sample shows a comparative sorption process for BS dye. According to correlation coefficient values for both adsorption isotherms, it can be suggested that the Freundlich model is the best model to fit the experimental data compared to the Langmuir model [43].

Thermodynamics Study

To estimate thermodynamic data, such as standard enthalpy changes ($\Delta H°$), standard entropy changes ($\Delta S°$),

Table 3. Maximum adsorption capacities reported in the literature for BS dye using various adsorbents

Adsorbent	q_m (mg/g)	Ref
Calcined metal layered double hydroxide Mg-Al-Cu-Fe-CO$_3$ (CLDH)	901.54	[32]
Metal layered double hydroxide Mg–Al–Cu–Fe–CO$_3$ (LDH)	107.31	[32]
Commercial gelatin/CNT's beads and recovered from chromium-tanned leather wastes (RCTLW) gelatin/CNT's	202.39, 131.32	[33]
Chromium and vegetable tanned leather waste (CTLW and VTLW)	73.52, 78.12	[8]
Layered double hydroxides Mg–Al–CO$_3$ LDH	102.70	[34]
Calcined layered double hydroxides Mg–Al CLDH	98.33	[34]
Green Microalgae *Acutodesmus obliquus* strain	44.24	[35]
Semi-IPN NaAla-Gel-cl-polyAAm	1.96	[36]
Cellulose-based sodium alginate/iron C/SA/Fe 0.25 g	67.98	[37]
Cellulose-based sodium alginate/iron C/SA/Fe 0.5 g	105.93	[37]
Cellulose-based sodium alginate/iron C/SA/Fe 1.0 g	63.49	[37]
Fe/FeC	15.53	[38]
FeC	13.92	[38]
Fe	8.62	[38]
TiO$_2$	1.42×10^{-5}	[39]
BT	4.88	This study
MT	5.35	This study
Ca-M	0.83	This study

388
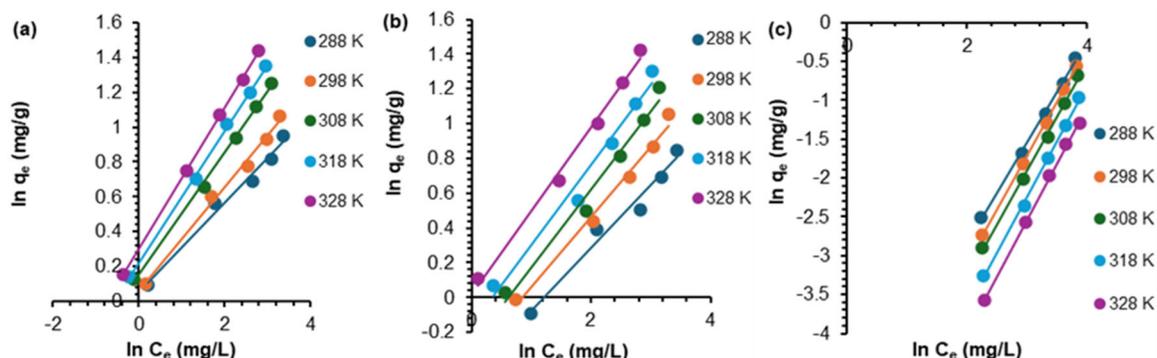
Indones. J. Chem., 2025, 25 (2), 381 - 393

Fig 8. Freundlich isotherm plots of BS dye adsorption onto (a) BT, (b) MT, and (c) Ca-M clay samples at different temperatures

Table 4. Freundlich isotherm constants for the adsorption of BS dye onto BT, MT, and Ca-M clay samples at different temperatures

Adsorbents	Temperature (K)	Slope ($1/n_f$)	n_f	Intercept (ln K_{Fr})	K_{Fr}	R^2
BT	288	0.2578	3.878976	0.0500	1.051271	0.9843
	298	0.2974	3.362475	0.2974	1.346354	0.9918
	308	0.3511	2.848191	0.1520	1.164160	0.9977
	318	0.3794	2.635741	0.2235	1.250446	0.9986
	328	0.4072	2.455796	0.2977	1.346758	0.9997
MT	288	0.3598	2.779322	−0.4343	0.647718	0.9750
	298	0.4034	2.478929	−0.3411	0.710988	0.9871
	308	0.4485	2.229654	−0.2733	0.760864	0.9792
	318	0.4608	2.170139	−0.1612	0.851122	0.9785
	328	0.4796	2.085071	0.0199	1.020099	0.9921
Ca-M	288	1.2968	0.771129	−5.4350	0.004361	0.9980
	298	1.3814	0.723903	−5.8517	0.002875	0.9989
	308	1.4043	0.712099	−6.1128	0.002214	0.9975
	318	1.4501	0.689608	−6.5856	0.001380	0.9979
	328	1.4534	0.688042	−6.8820	0.001026	0.9993

and Gibbs free energy ($\Delta G°$), the Eq. (6-9) were used [44-45];

$$\Delta G° = -RT\ln K_{eq} \tag{6}$$

$$K_{eq} = \frac{C_i - C_e}{C_e}\left[\frac{V}{m}\right] \tag{7}$$

$$\Delta G° = \Delta H° - T\Delta S° \tag{8}$$

$$\ln K_{eq} = \frac{\Delta S°}{R} - \frac{\Delta H°}{RT} \tag{9}$$

where R is the universal gas constant, K_{eq} is the equilibrium constant for the adsorption process, T is the absolute temperature (K), V is the BS solution's volume (L), m is the mass of the clay samples (g), and C_i and C_e are the initial and the equilibrium concentrations (mg/L)

of the adsorbate, respectively. The values of $\Delta S°$ and $\Delta H°$ were estimated from the intercept and slope of the Van't Hoff plot, as shown in Fig. 9. Table 5 contains values for the thermodynamic data for the BS dye adsorption onto BT, MT, and Ca-M clay samples. It is evident from Table 5 that when BT and MT clay samples were used as adsorbents, the values of $\Delta H°$ and $\Delta S°$ were negative, indicating that the adsorption process was an exothermic process with a decrease in the disorder at the solid-solution interface. In addition, the negative values of $\Delta G°$ for all adsorbents showed that the adsorption of BS dye onto clay samples was possible and spontaneous [13]. On the other hand, for the raw clay sorbent, the
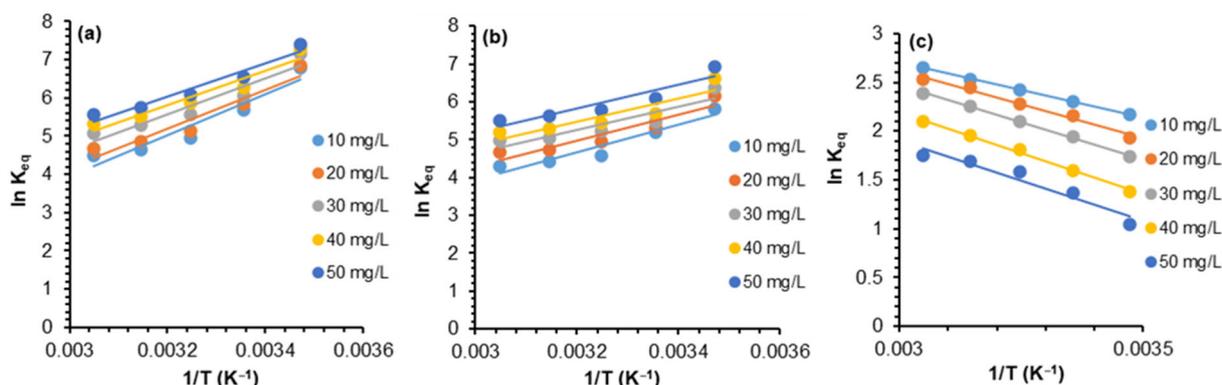
Fig 9. Van't Hoff plots for the adsorption of BS dye onto (a) BT, (b) MT, and (c) Ca-M clay samples

Table 5. Thermodynamic parameters for the adsorption of BS dye onto BT, MT, and Ca-M clay samples

Adsorbent	C_i (mg/L)	$\Delta H°$ (kJ/mol)	$\Delta S°$ (J/(mol K))	$-\Delta G°$ (kJ/mol)				
				288 K	298 K	308 K	318 K	328 K
BT	10	−44.9031	−101.955	16.2511	16.9660	18.3114	19.2754	20.2225
	20	−42.0846	−91.4291	13.6144	14.4408	15.4699	16.5894	17.8559
	30	−38.9885	−78.4093	11.8450	12.7444	14.2837	15.5296	16.6292
	40	−37.5219	−71.7698	11.1148	12.0337	13.5404	14.5644	15.6725
	50	−35.8034	−64.3346	10.7409	11.6106	12.9975	14.0394	15.1580
MT	10	−30.1358	−57.5803	1.39484	1.52534	1.63327	1.74551	1.88479
	20	−28.4372	−49.5880	1.24275	1.31704	1.40170	1.50055	1.66429
	30	−25.8740	−39.1116	1.09856	1.22777	1.34068	1.43829	1.57991
	40	−25.7659	−36.9657	1.05891	1.17092	1.29289	1.39621	1.53162
	50	−26.1816	−35.4060	1.03276	1.15635	1.27268	1.37121	1.50310
Ca-M	10	9.319994	50.4003	5.18642	4.78789	4.46698	3.65577	2.85926
	20	11.71858	57.00411	5.52695	5.34901	4.98159	4.22069	3.73139
	30	12.63894	58.47402	5.79470	5.64858	5.36698	4.79581	4.31581
	40	14.04401	60.39622	6.06234	6.07442	5.78040	5.16023	4.60652
	50	13.66572	56.82868	6.33854	6.26515	6.12467	5.54255	4.76820

positive values of $\Delta H°$ and $\Delta S°$ refer to the endothermic process that occurs with an increase in disorder at the adsorbent solution interface during the adsorption process [46]. The lower values of enthalpy change $\Delta H°$ indicated that the adsorption process is physisorption type.

Kinetics Study

The chemical pathways and possible rate-limiting stage for the adsorption of BS dye onto clay samples were investigated using two kinetic models: pseudo-first-order and pseudo-second-order model. The adsorption results were subjected to a kinetic analysis using these two models [30]. This study was carried out under the

following conditions: the adsorbent weight 0.2 g/25 mL, pH 7, and BS dye concentration 10 mg/L, and at 298 K.

Pseudo-first-order model

The pseudo-first-order model is given by the Eq. (10);

$$\ln(q_e - q_t) = \ln q_e - k_1 t \tag{10}$$

where k_1 is rate constant per min (min^{-1}), q_t adsorbed amount of adsorbate onto adsorbent at time t (mg/g), and q_e is the equilibrium adsorption capacity (mg/g). From the slope and intercept of the plot of ln ($q_e - q_t$) vs. t, in Fig. 10, the values of k_1 and q_e were determined [47]. Table 6 shows the values of rate constants for pseudo-first-order model. It is clear from Table 6 that the highest
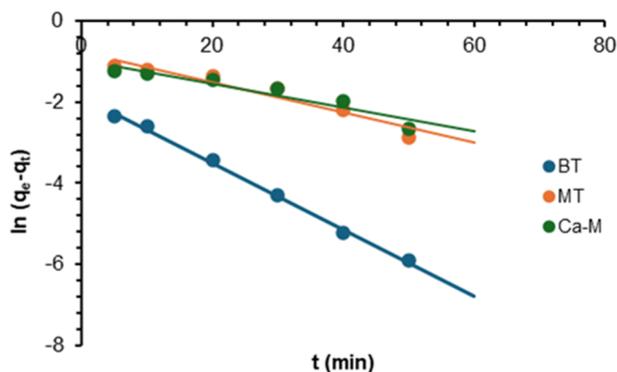
Fig 10. Pseudo-first-order model plot for the adsorption of BS dye onto BT, MT, and Ca-M clay samples at 298 K

Table 6. Pseudo-first-order model kinetic data for adsorption of BS dye onto BT, MT, and Ca-M clay samples at 298 K

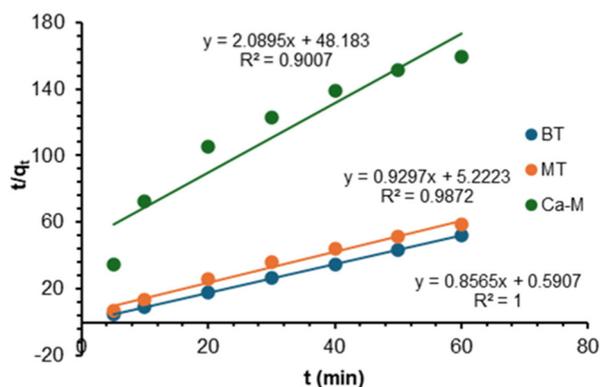| Adsorbent	$q_{e,exp}$ (mg/g)	$q_{e,cal}$ (mg/g)	k_1 (min^{-1})	R^2
BT	1.154506	0.156406	0.0821	0.9970
MT	1.154506	0.459232	0.0373	0.9264
Ca-M	1.154506	0.383966	0.0292	0.8993

Fig 11. Pseudo-second-order model plot for the adsorption of BS dye onto clay samples at 298 K

Table 7. Pseudo-second-order model kinetic data for adsorption of BS dye onto BT, MT, and Ca-M clay samples at 298 K

Adsorbent	$q_{e,exp}$ (mg/g)	$q_{e,cal}$ (mg/g)	k_1 (min^{-1})	R^2
BT	1.154506	1.167542	0.5907	1.0000
MT	1.025751	1.075616	5.2223	0.9872
Ca-M	0.432940	0.478583	48.183	0.9007

value of R^2 is 0.9970, and the lowest value of R^2 is 0.8993. Also, the calculated values of equilibrium adsorption capacity ($q_{e,cal}$) differ from the experimental $q_{e,exp}$ values.

This means that the pseudo-first-order kinetic model is adequately not applicable [48].

Pseudo-second-order model

The pseudo-second-order kinetic model is represented by Eq. (11);

$$\frac{t}{q_t} = \frac{1}{k_2 q_e^2} + \frac{t}{q_e} \tag{11}$$

where k_2 is the equilibrium rate constant for the pseudo-second-order (g/(mg min)). The values of k_2 and q_e can be obtained from the intercept and slope of the plot between $\frac{t}{q_t}$ vs. t, displayed in Fig. 11 [49]. Table 7 represents the pseudo-second-order model rate constants' values for the BS dye adsorption onto clay samples, according to the values of the regression coefficient R^2. Furthermore, the values of $q_{e,cal}$ are more closely with the $q_{e,exp}$ values for all clay samples, confirming that the pseudo-second-order kinetic model fits the experimental data better than the pseudo-first-order kinetic model [50].

■ CONCLUSION

In this research, BS dye was successfully removed from wastewater using Ca-montmorillonite clay and modified Ca-montmorillonite clay with two types of alkylammonium salts: MT and BT salts as adsorbent. The best adsorption isotherm model that fitted the equilibrium data was the Freundlich model. The maximum adsorption capacity values were increased after modification of the raw clay, indicating that using these salts enhanced the adsorption capacity of the raw clay. The adsorption of BS dye onto clay samples was found to be physisorption type. The adsorption process of this dye on the BT and MT clay surfaces was exothermic. A spontaneous process occurs with a decrease in disorder, while the dye adsorption onto raw clay is endothermic, and a spontaneous process occurs with an increase in disorder. Pseudo-second-order model better represented the kinetic data.

■ ACKNOWLEDGMENTS

Indones. J. Chem., 2025, 25 (2), 381 - 393

391

■ **CONFLICT OF INTEREST**

There is no conflict of interest to declare regarding this study.

■ **AUTHOR CONTRIBUTIONS**

All authors contributed equally and agreed to the final version of this manuscript.

■ **REFERENCES**

[1] Ahmed, M.A., Ahmed, M.A., and Mohamed, A.A., 2023, Synthesis, characterization and application of chitosan/graphene oxide/copper ferrite nanocomposite for the adsorptive removal of anionic and cationic dyes from wastewater, *RSC Adv.*, 13 (8), 5337–5352.

[2] Appiah-Brempong, M., Essandoh, H.M.K., Asiedu, N.Y., and Momade, F.Y., 2024, Bone char adsorption of COD and colour from tannery wastewater: Breakthrough curve analysis and fixed bed dynamic modelling, *Adv. Civ. Eng.*, 2024 (1), 6651094.

[3] Ramesh, B., Saravanan, A., Senthil Kumar, P., Yaashikaa, P.R., Thamarai, P., Shaji, A., and Rangasamy, G., 2023, A review on algae biosorption for the removal of hazardous pollutants from wastewater: Limiting factors, prospects and recommendations, *Environ. Pollut.*, 327, 121572.

[4] Hashemian, S., Sadeghi, B., Mozafari, F., Salehifar, H., and Salari, K., 2013, Adsorption of disperse of yellow 42 onto bentonite and organo-modified bentonite by tetra butyl ammonium iodide (B-TBAI), *Pol. J. Environ. Stud.*, 22 (5), 1363–1370.

[5] Tunç, S., Gürkan, T., and Duman, O., 2012, On-line spectrophotometric method for the determination of optimum operation parameters on the decolorization of Acid Red 66 and Direct Blue 71 from aqueous solution by Fenton process, *Chem. Eng. J.*, 181-182, 431–442.

[6] AbdulRazak, A.A., Shakor, Z.M., and Rohani, S., 2018, Optimizing Biebrich scarlet removal from water by magnetic zeolite 13X using response surface method, *J. Environ. Chem. Eng.*, 6 (5), 6175–6183.

[7] Tkaczyk, A., Mitrowska, K., and Posyniak, A., 2020, Synthetic organic dyes as contaminants of the aquatic environment and their implications for ecosystems: A review, *Sci. Total Environ.*, 717, 137222.

[8] AL-Shammari, N.H., and AL-Mammar, D.E., 2022, Adsorption of Biebrich scarlet dye into remains chromium and vegetable tanned leather as adsorbents, *Iraqi J. Sci.*, 63 (7), 2814–2826.

[9] Ouachtak, H., El Guerdaoui, A., El Haouti, R., Haounati, R., Ighnih, H., Toubi, Y., Alakhras, F., Rehman, R., Hafid, N., Addi, A.A., and Taha, M.L., 2023, Combined molecular dynamics simulations and experimental studies of the removal of cationic dyes on the eco-friendly adsorbent of activated carbon decorated montmorillonite Mt@AC, *RSC Adv.*, 13 (8), 5027–5044.

[10] Jiang, J.Q., and Ashekuzzaman, S.M., 2012, Development of novel inorganic adsorbent for water treatment, *Curr. Opin. Chem. Eng.*, 1 (2), 191–199.

[11] Chu, Y., Dai, Y., Xia, M., Xing, X., Wang, F., Li, Y., and Gao, H., 2024, The enhanced adsorption of diclofenac sodium (DCF) and ibuprofen (IBU) on modified montmorillonite with benzyldimethylhexadecylammonium chloride (HDBAC), *Colloids Surf., A*, 681, 132764.

[12] Zango, Z.U., Garba, A., Garba, Z.N., Zango, M.U., Usman, F., and Lim, J.W., 2022, Montmorillonite for adsorption and catalytic elimination of pollutants from wastewater: A state-of-the-arts review, *Sustainability*, 14 (24), 16441.

[13] Ali, O.S., and AL-Mammar, D.E., 2024, Adsorption of the color pollutant onto NiO nanoparticles prepared by a new green method, *Iraqi J. Sci.*, 65 (4), 1824–1838.

[14] Onukwuli, O.D., Obiora-Okafo, I.A., and Omotioma, M., 2019, Characterization and colour removal from an aqueous solution using bio-coagulants: Response surface methodological approach, *J. Chem. Technol. Metall.*, 54 (1), 77–89.

[15] Grigoraş, C.G., Simion, A.I., Favier, L., and Gavrilă, L., 2021, Effective removal of Biebrich scarlet dye from aqueous solutions by adsorption on cherry stones powder coated with chitosan, *2021 International Conference on e-Health and Bioengineering*, 18-19 November 2021, Iasi, Romania.

[16] Bwatanglang, I.B., Magili, S.T., and Kaigamma, I., 2021, Adsorption of phenol over bio-based

392

Indones. J. Chem., 2025, 25 (2), 381 - 393

silica/calcium carbonate (CS-SiO$_2$/CaCO$_3$) nanocomposite synthesized from waste eggshells and rice husks, *PeerJ Phys. Chem.*, 3, e17.

[17] Al-Wadi, A.M., and Al-Mammar, D.E., 2022, Green synthesis by *Zygophyllum coccineum* leaves extract for preparing ZnO nanoparticles, and characteristics study, *Egypt. J. Chem.*, 65 (5), 363–369.

[18] Tyagi, B., Chudasama, C.D., and Jasra, R.V., 2006, Determination of structural modification in acid activated montmorillonite clay by FT-IR spectroscopy, *Spectrochim. Acta, Part A*, 64 (2), 273–278.

[19] Lou, Y., Schapman, D., Mercier, D., Alexandre, S., Burel, F., Thebault, P., and Kébir, N., 2021, Preparation of bactericidal surfaces with high quaternary ammonium content through photo-initiated polymerization of *N*-[2-(acryloyloxy) ethyl]-*N*,*N*-dimethyl-*N*-butylammonium iodide from native and thiolated PDMS surfaces, *React. Funct. Polym.*, 165, 104941.

[20] Wu, P., Wu, W., Li, S., Xing, N., Zhu, N., Li, P., Wu, J., Yang, C., and Dang, Z., 2009, Removal of Cd^{2+} from aqueous solution by adsorption using Fe-montmorillonite, *J. Hazard. Mater.*, 169 (1), 824–830.

[21] Khan, S., Ajmal, S., Hussain, T., and Rahman, M.U., 2023, Clay-based materials for enhanced water treatment: Adsorption mechanisms, challenges, and future directions, *J. Umm Al-Qura Univ. Appl. Sci.*, 9 (3), 1–16.

[22] Egbosiuba, T.C., Tran, T.Q., Arole, K., Zhang, Y., Enyoh, C.E., Mustapha, S., Tijani, J.O., Yadav, V.K., Anadebe, V.C., and Abdulkareem, A.S., 2024, Biotreatment of clay-based adsorbent to eliminate arsenic (V) ions and malachite green from wastewater: Isotherm, kinetics, thermodynamics, reusability and mechanism, *Results Eng.*, 22, 102073.

[23] Rápó, E., and Tonk, S., 2021, Factors affecting synthetic dye adsorption; desorption studies: A review of results from the last five years (2017–2021), *Molecules*, 26 (17), 5419.

[24] Rafatullah, M., Sulaiman, O., Hashim, R., and Ahmad, A., 2009, Adsorption of copper(II), chromium(III), nickel(II) and lead(II) ions from aqueous solutions by meranti sawdust, *J. Hazard. Mater.*, 170 (2), 969–977.

[25] Al-Saade, K.A.S., AL-Mammar, D.E., and AL-Ani, H.N., 2017, Using *Phragmites australis* (Iraqi plant) to remove the lead(II) Ions form aqueous solution, *Baghdad Sci. J.*, 14 (1), 0148.

[26] Aljeboree, A.M., and Alkaim, A.F., 2024, Studying removal of anionic dye by prepared highly adsorbent surface hydrogel nanocomposite as an applicable for aqueous solution, *Sci. Rep.*, 14 (1), 9102.

[27] AL-Mammar, D.E., 2024, Adsorption of Brilliant scarlet 3R dye onto corn silk as agricultural waste in neutral medium, *Iraqi J. Sci.*, 65 (7), 3606–3619.

[28] Zaghloul, A., Ichou, A.A., Abali, M.H., Benhiti, R., Soudani, A., Carja, G., Chiban, M., Zerbet, M., and Sinan, F., 2021, Removal and comparative adsorption of anionic dye on various MgAl synthetic clay, *Biointerface Res. Appl. Chem.*, 11 (6), 14986–14997.

[29] Tun, H., and Chen, C.C., 2021, Isosteric heat of adsorption from thermodynamic Langmuir isotherm, *Adsorption*, 27 (6), 979–989.

[30] Wekoye, J.N., Wanyonyi, W.C., Wangila, P.T., and Tonui, M.K., 2020, Kinetic and equilibrium studies of Congo red dye adsorption on cabbage waste powder, *Environ. Chem. Ecotoxicol.*, 2, 24–31.

[31] Nakas, G.I., and Kaynak, C., 2009, Use of different alkylammonium salts in clay surface modification for epoxy-based nanocomposites, *Polym. Compos.*, 30 (3), 357–363.

[32] Harizi, I., Chebli, D., Bouguettoucha, A., Rohani, S., and Amrane, A., 2019, A new Mg–Al–Cu–Fe-LDH composite to enhance the adsorption of acid red 66 dye: Characterization, kinetics and isotherm analysis, *Arabian J. Sci. Eng.*, 44 (6), 5245–5261.

[33] Rigueto, C.V.T., Alessandretti, I., Rosseto, M., Geraldi, C.A.Q., Loss, R.A., Pizzutti, I.R., Piccin, J.S., and Dettmer, A., 2022, Tannery wastes-derived gelatin and carbon nanotubes composite beads: Adsorption and reuse studies using tartrazine yellow dye, *Matéria*, 27 (2), e13208.

[34] Chebli, D., Bouguettoucha, A., Reffas, A., Tiar, C., Boutahala, M., Gulyas, H., and Amrane, A., 2016, Removal of the anionic dye Biebrich scarlet from water by adsorption to calcined and non-calcined Mg–Al layered double hydroxides, *Desalin. Water*

Treat., 57 (46), 22061–22073.

[35] Sarwa, P., Vijayakumar, R., and Verma, S.K., 2014, Adsorption of acid red 66 dye from aqueous solution by green microalgae *Acutodesmus obliquus* strain PSV2 isolated from an industrial polluted site, *Open Access Lib. J.*, 1 (3), 1–8.

[36] Priya, P., Sharma, A.K., Kaith, B.S., Tanwar, V., Bhatia, J.K., Sharma, N., Bajaj, S., and Panchal, S., 2019, RSM-CCD optimized sodium alginate/gelatin based ZnS-nanocomposite hydrogel for the effective removal of Biebrich scarlet and crystal violet dyes, *Int. J. Biol. Macromol.*, 129, 214–226.

[37] Fang, Y., Liu, Q., and Zhu, S., 2021, Selective biosorption mechanism of methylene blue by a novel and reusable sugar beet pulp cellulose/sodium alginate/iron hydroxide composite hydrogel, *Int. J. Biol. Macromol.*, 188, 993–1002.

[38] Paz, C.B., Araújo, R.S., Oton, L.F., Oliveira, A.C., Soares, J.M., Medeiros, S.N., Rodríguez-Castellón, E., and Rodríguez-Aguado, E., 2020, Acid red 66 dye removal from aqueous solution by Fe/C-based composites: Adsorption, kinetics and thermodynamic studies, *Materials*, 13 (5), 1107.

[39] Mir, N.A., Khan, A., Dar, A.A., and Muneer, M., 2014, Photocatalytic study of two azo dye derivatives, ponceau bs and reactive blue 160 in aqueous suspension of TiO₂: Adsorption isotherm and decolorization kinetics, *IJIRSET*, 3 (2), 933–9348.

[40] Saed, S.A., and AL-Mammar, D.E., 2021, Influence of acid activation of a mixture of illite, koalinite, and chlorite clays on the adsorption of methyl violet 6B dye, *Iraqi J. Sci.*, 62 (6), 1761–1778.

[41] Abdul Salim, N.A., Puteh, M.H., Khamidun, M.H., Fulazzaky, M.A., Abdullah, N.H., Mohd Yusoff, A.R., Ahmad Zaini, M.A., Ahmad, N., Mat Lazim, Z., and Nuid, M., 2021, Interpretation of isotherm models for adsorption of ammonium onto granular activated carbon, *Biointerface Res. Appl. Chem.*, 11 (2), 9227–9241.

[42] Dada, A.O., Olalekan., A.P., Olatunya, A.M., and Dada, O., 2012, Langmuir, Freundlich, Temkin and Dubinin–Radushkevich isotherms studies of

equilibrium sorption of Zn²⁺ unto phosphoric acid modified rice husk, *IOSR J. Appl. Chem.*, 3 (1), 38–45.

[43] Mohammed, R.A., and Al-Mammar, D.E., 2019, Using tobacco leaves as adsorbent for the orange-G dye removal from its aqueous solutions, *J. Global Pharma Technol.*, 11, 273–280.

[44] Al-Mousawi, I.M.H., Khudhair, N.A., and Ahmed, L.S., 2022, DFT-quantum chemical and experimental studies of a new 2-(substituted thio) furan as a corrosion inhibitor in acidic media, *Nano Biomed. Eng.*, 14 (2), 136–148.

[45] Salim, R.T., and AL-Mammar, D.E., 2023, Adsorption of azo dye onto TiO₂ nanoparticles prepared by a novel green method: Isotherm and thermodynamic study, *Iraqi J. Sci.*, 64 (8), 3779–3792.

[46] Al-Asadi, S.T., Al-Qaim, F.F., Al-Saedi, H.F.S., Deyab, I.F., Kamyab, H., and Chelliapan, S., 2023, Adsorption of methylene blue dye from aqueous solution using low-cost adsorbent: kinetic, isotherm adsorption, and thermodynamic studies, *Environ. Monit. Assess.*, 195 (6), 676.

[47] Kajjumba, G.W., Emik, S., Öngen, A., Özcan, H.K., and Aydın, S., 2018, "Modelling of Adsorption Kinetic Processes—Errors, Theory and Application" in *Advanced Sorption Process Applications*, Eds. Edebali, S., IntechOpen, Rijeka, Croatia.

[48] AL-Shammari, N.H., and AL-Mammar, D.E., 2022, Equilibrium and kinetic modeling studies for the adsorption-desorption of methyl violet 10B onto leather waste, *Eurasian Chem. Commun.*, 4 (2), 175–189.

[49] Mekonnen, D.T., Alemayehu, E., and Lennartz, B., 2021, Adsorptive removal of phosphate from aqueous solutions using low-cost volcanic rocks: Kinetics and equilibrium approaches, *Materials*, 14 (5), 1312.

[50] Abaas, A.K., Al-Mammar, D.E., and Abbas, H.A., 2009, Equilibrium, thermodynamic and kinetic study of the adsorption of a new mono azo dye onto natural Iraq clay, *J. Global Pharma Technol.*, 10 (5), 102–109.